Eur. Phys. J. C 31, 149–164 (2003)
Digital Object Identifier (DOI) 10.1140/epjc/s2003-01358-2

THE EUROPEAN PHYSICAL JOURNAL C

Jet production in charged current deep inelastic e^+p scattering at HERA

The ZEUS Collaboration

S. Chekanov, M. Derrick, D. Krakauer, J.H. Loizides[1], S. Magill, B. Musgrave, J. Repond, R. Yoshida
Argonne National Laboratory, Argonne, Illinois 60439-4815, USA[n]

M.C.K. Mattingly
Andrews University, Berrien Springs, Michigan 49104-0380, USA

P. Antonioli, G. Bari, M. Basile, L. Bellagamba, D. Boscherini, A. Bruni, G. Bruni, G. Cara Romeo, L. Cifarelli, F. Cindolo, A. Contin, M. Corradi, S. De Pasquale, P. Giusti, G. Iacobucci, A. Margotti, R. Nania, F. Palmonari, A. Pesci, G. Sartorelli, A. Zichichi
University and INFN Bologna, Bologna, Italy[e]

G. Aghuzumtsyan, D. Bartsch, I. Brock, S. Goers, H. Hartmann, E. Hilger, P. Irrgang, H.-P. Jakob, A. Kappes[2], U.F. Katz[2], O. Kind, U. Meyer, E. Paul[3], J. Rautenberg, R. Renner, A. Stifutkin, J. Tandler, K.C. Voss, M. Wang, A. Weber[4]
Physikalisches Institut der Universität Bonn, Bonn, Germany[b]

D.S. Bailey[5], N.H. Brook[5], J.E. Cole, B. Foster, G.P. Heath, H.F. Heath, S. Robins, E. Rodrigues[6], J. Scott, R.J. Tapper, M. Wing
H.H. Wills Physics Laboratory, University of Bristol, Bristol, UK[m]

M. Capua, A. Mastroberardino, M. Schioppa, G. Susinno
Calabria University, Physics Department and INFN, Cosenza, Italy[e]

J.Y. Kim, Y.K. Kim, J.H. Lee, I.T. Lim, M.Y. Pac[7]
Chonnam National University, Kwangju, Korea[g]

A. Caldwell[8], M. Helbich, X. Liu, B. Mellado, Y. Ning, S. Paganis, Z. Ren, W.B. Schmidke, F. Sciulli
Nevis Laboratories, Columbia University, Irvington on Hudson, New York 10027, USA[o]

J. Chwastowski, A. Eskreys, J. Figiel, K. Olkiewicz, P. Stopa, L. Zawiejski
Institute of Nuclear Physics, Cracow, Poland[i]

L. Adamczyk, T. Bołd, I. Grabowska-Bołd, D. Kisielewska, A.M. Kowal, M. Kowal, T. Kowalski, M. Przybycień, L. Suszycki, D. Szuba, J. Szuba[9]
Faculty of Physics and Nuclear Techniques, University of Mining and Metallurgy, Cracow, Poland[p]

A. Kotański[10], W. Słomiński[11]
Department of Physics, Jagellonian University, Cracow, Poland

V. Adler, L.A.T. Bauerdick[12], U. Behrens, I. Bloch, K. Borras, V. Chiochia, D. Dannheim, G. Drews, J. Fourletova, U. Fricke, A. Geiser, F. Goebel[8], P. Göttlicher[13], O. Gutsche, T. Haas, W. Hain, G.F. Hartner, S. Hillert, B. Kahle, U. Kötz, H. Kowalski[14], G. Kramberger, H. Labes, D. Lelas, B. Löhr, R. Mankel, I.-A. Melzer-Pellmann, M. Moritz[15], C.N. Nguyen, D. Notz, M.C. Petrucci[16], A. Polini, A. Raval, U. Schneekloth, F. Selonke[3], U. Stoesslein, H. Wessoleck, G. Wolf, C. Youngman, W. Zeuner
Deutsches Elektronen-Synchrotron DESY, Hamburg, Germany

S. Schlenstedt
DESY Zeuthen, Zeuthen, Germany

G. Barbagli, E. Gallo, C. Genta, P. G. Pelfer
University and INFN, Florence, Italy[e]

A. Bamberger, A. Benen, N. Coppola
Fakultät für Physik der Universität Freiburg i.Br., Freiburg i.Br., Germany[b]

M. Bell, P.J. Bussey, A.T. Doyle, C. Glasman, J. Hamilton, S. Hanlon, S.W. Lee, A. Lupi, D.H. Saxon, I.O. Skillicorn
Department of Physics and Astronomy, University of Glasgow, Glasgow, UK[m]

I. Gialas
Department of Engineering in Management and Finance, Univ. of Aegean, Greece

B. Bodmann, T. Carli, U. Holm, K. Klimek, N. Krumnack, E. Lohrmann, M. Milite, H. Salehi, S. Stonjek[17], K. Wick, A. Ziegler, Ar. Ziegler
Hamburg University, Institute of Exp. Physics, Hamburg, Germany[b]

C. Collins-Tooth, C. Foudas, R. Gonçalo[6], K.R. Long, A.D. Tapper
Imperial College London, High Energy Nuclear Physics Group, London, UK[m]

P. Cloth, D. Filges
Forschungszentrum Jülich, Institut für Kernphysik, Jülich, Germany

K. Nagano, K. Tokushuku[18], S. Yamada, Y. Yamazaki
Institute of Particle and Nuclear Studies, KEK, Tsukuba, Japan[f]

A.N. Barakbaev, E.G. Boos, N.S. Pokrovskiy, B.O. Zhautykov
Institute of Physics and Technology of Ministry of Education and Science of Kazakhstan, Almaty, Kazakhstan

H. Lim, D. Son
Kyungpook National University, Taegu, Korea[g]

K. Piotrzkowski
Institut de Physique Nucléaire, Université Catholique de Louvain, Louvain-la-Neuve, Belgium

F. Barreiro, O. González, L. Labarga, J. del Peso, E. Tassi, J. Terrón, M. Vázquez
Departamento de Física Teórica, Universidad Autónoma de Madrid, Madrid, Spain[l]

M. Barbi, F. Corriveau, S. Gliga, J. Lainesse, S. Padhi, D.G. Stairs
Department of Physics, McGill University, Montréal, Québec, Canada H3A 2T8[a]

T. Tsurugai
Meiji Gakuin University, Faculty of General Education, Yokohama, Japan[f]

A. Antonov, P. Danilov, B.A. Dolgoshein, D. Gladkov, V. Sosnovtsev, S. Suchkov
Moscow Engineering Physics Institute, Moscow, Russia[j]

R.K. Dementiev, P.F. Ermolov, Yu.A. Golubkov, I.I. Katkov, L.A. Khein, I.A. Korzhavina, V.A. Kuzmin, B.B. Levchenko[19], O.Yu. Lukina, A.S. Proskuryakov, L.M. Shcheglova, N.N. Vlasov, S.A. Zotkin
Moscow State University, Institute of Nuclear Physics, Moscow, Russia[k]

N. Coppola, S. Grijpink, E. Koffeman, P. Kooijman, E. Maddox, A. Pellegrino, S. Schagen, H. Tiecke, J.J. Velthuis, L. Wiggers, E. de Wolf
NIKHEF and University of Amsterdam, Amsterdam, The Netherlands[h]

N. Brümmer, B. Bylsma, L.S. Durkin, T.Y. Ling
Physics Department, Ohio State University, Columbus, Ohio 43210, USA[n]

A.M. Cooper-Sarkar, A. Cottrell, R.C.E. Devenish, J. Ferrando, G. Grzelak, S. Patel, M.R. Sutton, R. Walczak
Department of Physics, University of Oxford, Oxford, UK[m]

A. Bertolin, R. Brugnera, R. Carlin, F. Dal Corso, S. Dusini, A. Garfagnini, S. Limentani, A. Longhin, A. Parenti, M. Posocco, L. Stanco, M. Turcato
Dipartimento di Fisica dell' Università and INFN, Padova, Italy[e]

E.A. Heaphy, F. Metlica, B.Y. Oh, J.J. Whitmore[20]
Department of Physics, Pennsylvania State University, University Park, Pennsylvania 16802, USA[o]

Y. Iga
Polytechnic University, Sagamihara, Japan[f]

G. D'Agostini, G. Marini, A. Nigro
Dipartimento di Fisica, Università 'La Sapienza' and INFN, Rome, Italy [e]

C. Cormack[21], J.C. Hart, N.A. McCubbin
Rutherford Appleton Laboratory, Chilton, Didcot, Oxon, UK[m]

C. Heusch
University of California, Santa Cruz, California 95064, USA[n]

I.H. Park
Department of Physics, Ewha Womans University, Seoul, Korea

N. Pavel
Fachbereich Physik der Universität-Gesamthochschule Siegen, Germany

H. Abramowicz, A. Gabareen, S. Kananov, A. Kreisel, A. Levy
Raymond and Beverly Sackler Faculty of Exact Sciences, School of Physics, Tel-Aviv University, Tel-Aviv, Israel[d]

M. Kuze
Department of Physics, Tokyo Institute of Technology, Tokyo, Japan[f]

T. Abe, T. Fusayasu, S. Kagawa, T. Kohno, T. Tawara, T. Yamashita
Department of Physics, University of Tokyo, Tokyo, Japan[f]

R. Hamatsu, T. Hirose[3], M. Inuzuka, S. Kitamura[22], K. Matsuzawa, T. Nishimura
Tokyo Metropolitan University, Department of Physics, Tokyo, Japan[f]

M. Arneodo[23], M.I. Ferrero, V. Monaco, M. Ruspa, R. Sacchi, A. Solano
Università di Torino, Dipartimento di Fisica Sperimentale and INFN, Torino, Italy[e]

T. Koop, G.M. Levman, J.F. Martin, A. Mirea
Department of Physics, University of Toronto, Toronto, Ontario, Canada M5S 1A7[a]

J.M. Butterworth, C. Gwenlan, R. Hall-Wilton, T.W. Jones, M.S. Lightwood, B.J. West
Physics and Astronomy Department, University College London, London, UK[m]

J. Ciborowski[24], R. Ciesielski[25], R.J. Nowak, J.M. Pawlak, J. Sztuk[26], T. Tymieniecka[27], A. Ukleja[27], J. Ukleja, A.F. Żarnecki
Warsaw University, Institute of Experimental Physics, Warsaw, Poland[q]

M. Adamus, P. Plucinski
Institute for Nuclear Studies, Warsaw, Poland[q]

Y. Eisenberg, L.K. Gladilin[28], D. Hochman, U. Karshon, M. Riveline
Department of Particle Physics, Weizmann Institute, Rehovot, Israel[c]

D. Kçira, S. Lammers, L. Li, D.D. Reeder, A.A. Savin, W.H. Smith
Department of Physics, University of Wisconsin, Madison, Wisconsin 53706, USA[n]

A. Deshpande, S. Dhawan, P.B. Straub
Department of Physics, Yale University, New Haven, Connecticut 06520-8121, USA[n]

S. Bhadra, C.D. Catterall, S. Fourletov, G. Hartner, S. Menary, M. Soares, J. Standage
Department of Physics, York University, Ontario, Canada M3J 1P3[a]

[1] also affiliated with University College London
[2] on leave of absence at University of Erlangen-Nürnberg, Germany
[3] retired
[4] self-employed
[5] PPARC Advanced fellow
[6] supported by the Portuguese Foundation for Science and Technology (FCT)
[7] now at Dongshin University, Naju, Korea
[8] now at Max-Planck-Institut für Physik, München/Germany
[9] partly supported by the Israel Science Foundation and the Israel Ministry of Science
[10] supported by the Polish State Committee for Scientific Research, grant no. 2 P03B 09322
[11] member of Dept. of Computer Science
[12] now at Fermilab, Batavia/IL, USA
[13] now at DESY group FEB
[14] on leave of absence at Columbia Univ., Nevis Labs., N.Y./USA
[15] now at CERN
[16] now at INFN Perugia, Perugia, Italy
[17] now at Univ. of Oxford, Oxford/UK
[18] also at University of Tokyo
[19] partly supported by the Russian Foundation for Basic Research, grant 02-02-81023

[20] on leave of absence at The National Science Foundation, Arlington, VA/USA
[21] now at Univ. of London, Queen Mary College, London, UK
[22] present address: Tokyo Metropolitan University of Health Sciences, Tokyo 116-8551, Japan
[23] also at Università del Piemonte Orientale, Novara, Italy
[24] also at Łódź University, Poland
[25] supported by the Polish State Committee for Scientific Research, grant no. 2 P03B 07222
[26] Łódź University, Poland
[27] supported by German Federal Ministry for Education and Research (BMBF), POL 01/043
[28] on leave from MSU, partly supported by University of Wisconsin via the U.S.-Israel BSF

Received: 5 June 2003 /
Published online: 10 October 2003 – © Springer-Verlag / Società Italiana di Fisica 2003

Abstract. The production rates and substructure of jets have been studied in charged current deep inelastic e^+p scattering for $Q^2 > 200$ GeV^2 with the ZEUS detector at HERA using an integrated luminosity of 110.5 pb^{-1}. Inclusive jet cross sections are presented for jets with transverse energies $E_T^{\rm jet} > 14$ GeV and pseudorapidities in the range $-1 < \eta^{\rm jet} < 2$. Dijet cross sections are presented for events with a jet having $E_T^{\rm jet} > 14$ GeV and a second jet having $E_T^{\rm jet} > 5$ GeV. Measurements of the mean subjet multiplicity, $\langle n_{\rm sbj}\rangle$, of the inclusive jet sample are presented. Predictions based on parton-shower Monte Carlo models and next-to-leading-order QCD calculations are compared to the measurements. The value of $\alpha_s(M_Z)$, determined from $\langle n_{\rm sbj}\rangle$ at $y_{\rm cut} = 10^{-2}$ for jets with $25 < E_T^{\rm jet} < 119$ GeV, is $\alpha_s(M_Z) = 0.1202 \pm 0.0052\,({\rm stat.})\,^{+0.0060}_{-0.0019}\,({\rm syst.})\,^{+0.0065}_{-0.0053}\,({\rm th.})$. The mean subjet multiplicity as a function of Q^2 is found to be consistent with that measured in NC DIS.

1 Introduction

Measurements of the charged current (CC) deep inelastic scattering (DIS) cross section at HERA [1–9] at high virtuality, Q^2, of the exchanged boson have demonstrated the presence of a space-like propagator with a finite mass, consistent with that of the W boson. Jet production in CC DIS provides a testing ground for QCD as well as the electroweak sector of the Standard Model. Up to leading order in the strong coupling constant, α_s, jet production in CC DIS proceeds via the QCD-Compton ($Wq \to q'g$) and W-gluon-fusion ($Wg \to q\bar{q}'$) processes in addition to the pure electroweak process ($Wq \to q'$).

At HERA, multijet structure has been observed in CC DIS [5,10] at large Q^2 and jet substructure has been studied using the differential and integrated jet shapes [11]. Another useful representation of the internal jet structure is the subjet multiplicity [12–15]. The lowest-order non-trivial contribution to the subjet multiplicity is of order α_s, so that measurements of the subjet multiplicity provide a direct test of QCD.

This paper reports a detailed study of the hadronic final state in CC e^+p DIS. Differential cross sections are presented for both inclusive jet and dijet production. The jets were identified in the laboratory frame using the longitudinally invariant k_T cluster algorithm [16]. After describing experimental conditions and the theoretical calculations, in Sect. 7.2 the inclusive jet cross sections are presented as a function of the virtuality of the exchanged boson, the jet

[a] supported by the Natural Sciences and Engineering Research Council of Canada (NSERC)
[b] supported by the German Federal Ministry for Education and Research (BMBF), under contract numbers HZ1GUA 2, HZ1GUB 0, HZ1PDA 5, HZ1VFA 5
[c] supported by the MINERVA Gesellschaft für Forschung GmbH, the Israel Science Foundation, the U.S.-Israel Binational Science Foundation and the Benozyio Center for High Energy Physics
[d] supported by the German-Israeli Foundation and the Israel Science Foundation
[e] supported by the Italian National Institute for Nuclear Physics (INFN)
[f] supported by the Japanese Ministry of Education, Culture, Sports, Science and Technology (MEXT) and its grants for Scientific Research
[g] supported by the Korean Ministry of Education and Korea Science and Engineering Foundation
[h] supported by the Netherlands Foundation for Research on Matter (FOM)
[i] supported by the Polish State Committee for Scientific Research, grant no. 620/E-77/SPUB-M/DESY/P-03/DZ 247/2000-2002
[j] partially supported by the German Federal Ministry for Education and Research (BMBF)
[k] supported by the Fund for Fundamental Research of Russian Ministry for Science and Education and by the German Federal Ministry for Education and Research (BMBF)
[l] supported by the Spanish Ministry of Education and Science through funds provided by CICYT
[m] supported by the Particle Physics and Astronomy Research Council, UK
[n] supported by the US Department of Energy
[o] supported by the US National Science Foundation
[p] supported by the Polish State Committee for Scientific Research, grant no. 112/E-356/SPUB-M/DESY/P-03/DZ 301/2000-2002, 2 P03B 13922
[q] supported by the Polish State Committee for Scientific Research, grant no. 115/E-343/SPUB-M/DESY/P-03/DZ 121/2001-2002, 2 P03B 07022

pseudorapidity, $\eta^{\rm jet}$, and the jet transverse energy, $E_T^{\rm jet}$. In Sect. 7.3, the dependence of the dijet cross sections on Q^2 and the invariant mass, m_{12}, of the two highest-E_T jets are given. In Sect. 7.4, the mean subjet multiplicity, $\langle n_{\rm sbj}\rangle$, as a function of the resolution scale, $y_{\rm cut}$ and $E_T^{\rm jet}$ using the inclusive jet sample is presented. Parton-shower Monte Carlo (MC) calculations and next-to-leading-order (NLO) QCD predictions [17] are compared to the measurements. In Sect. 8, the value of $\alpha_s(M_Z)$ determined using the measurements of $\langle n_{\rm sbj}\rangle$ as a function of $E_T^{\rm jet}$ is given. In Sect. 9, the measurements of $\langle n_{\rm sbj}\rangle$ as a function of $E_T^{\rm jet}$ and Q^2 are compared to the results obtained by ZEUS in neutral current (NC) DIS [18].

2 Experimental conditions

The data sample used in this analysis was collected with the ZEUS detector at HERA and corresponds to an integrated luminosity of 110.5 pb^{-1}. During the 1995-1997 (1999-2000) running period, HERA operated with protons of energy $E_p = 820$ GeV (920 GeV) and positrons of energy $E_e = 27.5$ GeV, yielding a centre-of-mass energy of 300 GeV (318 GeV). A detailed description of the ZEUS detector can be found elsewhere [19]. A brief outline of the components that are most relevant for this analysis is given below. Charged particles are tracked in the central tracking detector (CTD) [20–22], which operates in a magnetic field of 1.43 T provided by a thin superconducting solenoid. The CTD consists of 72 cylindrical drift chamber layers, organized in nine superlayers covering the polar-angle[1] region $15^\circ < \theta < 164^\circ$. The transverse-momentum resolution for full-length tracks is $\sigma(p_T)/p_T = 0.0058p_T \oplus 0.0065 \oplus 0.0014/p_T$, with p_T in GeV. The high-resolution uranium-scintillator calorimeter (CAL) [23–26] consists of three parts: the forward (FCAL), the barrel (BCAL) and the rear (RCAL) calorimeters. Each part is subdivided transversely into towers and longitudinally into one electromagnetic section (EMC) and either one (in RCAL) or two (in BCAL and FCAL) hadronic sections (HAC). The smallest subdivision of the calorimeter is called a cell. The CAL energy resolutions, as measured under test-beam conditions, are $\sigma(E)/E = 0.18/\sqrt{E}$ for electrons and $\sigma(E)/E = 0.35/\sqrt{E}$ for hadrons, with E in GeV. Jet energies were corrected for the energy lost in inactive material, typically about one radiation length, in front of the CAL. The effects of the uranium noise were minimised by discarding cells in the electromagnetic or hadronic sections if they had energy deposits of less than 60 MeV or 110 MeV, respectively. A three-level trigger [19,27] was used to select events online.

[1] The ZEUS coordinate system is a right-handed Cartesian system, with the Z axis pointing in the proton beam direction, referred to as the "forward direction", and the X axis pointing left towards the centre of HERA. The coordinate origin is at the nominal interaction point. The pseudorapidity is defined as $\eta = -\ln\left(\tan\frac{\theta}{2}\right)$, where the polar angle, θ, is measured with respect to the proton beam direction.

The luminosity was measured using the Bethe-Heitler reaction $e^+p \to e^+p\gamma$. The resulting small-angle energetic photons were measured by the luminosity monitor [28–30], a lead-scintillator calorimeter placed in the HERA tunnel at $Z = -107$ m.

3 Data selection and jet search

The selection of charged current events for the present study is very similar to those described in detail in previous ZEUS publications [6,7]. The efficiency of the selection cuts is typically above 90% and the remaining backgrounds are negligible.

The principal signature of a CC DIS event at HERA is the presence of a large missing transverse momentum, $\not{p}_T$, arising from the energetic final-state neutrino which escapes detection. The quantity $\not{p}_T$ was calculated from

$$\not{p}_T{}^2 = p_X^2 + p_Y^2 = \left(\sum_i E_i \sin\theta_i \cos\phi_i\right)^2 + \left(\sum_i E_i \sin\theta_i \sin\phi_i\right)^2,$$

where the sums run over all CAL cells, i, E_i is the energy deposit and θ_i, ϕ_i are the polar and azimuthal angles of the cell as viewed from the interaction vertex. The total transverse energy, E_T, is given by $E_T = \sum E_i \sin\theta_i$.

The inelasticity, y, was reconstructed using the Jacquet-Blondel method [31] and corrected for detector effects as described previously [5]. The detector simulation was used to derive corrected values $\not{p}_{T,\rm cor}$ and $y_{\rm cor}$. The corrected value of Q^2, $Q^2_{\rm cor}$, was calculated in terms of $\not{p}_{T,\rm cor}$ and $y_{\rm cor}$ using the relation $Q^2_{\rm cor} = \not{p}^2_{T,\rm cor}/(1-y_{\rm cor})$.

The following requirements were imposed on the data sample:

- $\not{p}_T > 11$ GeV and $Q^2_{\rm cor} > 200$ GeV^2, to ensure high trigger efficiency;
- $y_{\rm cor} < 0.9$, to avoid the degradation of the resolution in Q^2 near $y \sim 1$;
- $\not{p}_T/E_T > 0.5$, to reject photoproduction and beam-gas background. For the dijet sample, this cut was reduced to $\not{p}_T/E_T > 0.3$ with the further requirement that the difference between the azimuthal angle of the missing transverse momentum and that of the closest jet was greater than 1 rad. This cut removed poorly reconstructed back-to-back dijet photoproduction events;
- a vertex position reconstructed with the CTD in the range $-50 < Z < 50$ cm, consistent with an ep interaction;
- the difference, $\Delta\phi$, between the azimuthal angle of the net transverse momentum as measured by the tracks associated with the vertex and that measured from the CAL be less than 1 rad. This requirement removed random coincidences of cosmic rays with ep interactions;
- $p_T^{\rm track}/\not{p}_T > 0.1$, where $p_T^{\rm track}$ is the net transverse momentum of the tracks associated with the vertex. This condition was not applied if $\not{p}_T > 25$ GeV. This cut rejected events with additional energy deposits in the

CAL not related to ep interactions (mainly cosmic rays) and beam-related background in which $\not{p}_T$ has a small polar angle;
- the event was removed from the sample if there was an isolated positron candidate with energy above 10 GeV, to reject NC DIS events;
- a pattern-recognition algorithm based on the topology of the calorimeter energy distribution and the signals detected in the muon chambers was applied to reject cosmic rays and beam-halo muons.

The longitudinally invariant k_T cluster algorithm [16] was used in the inclusive mode [32] to reconstruct jets in the hadronic final state both in data and in MC simulated events (see Sect. 4). In data and MC, the algorithm was applied to the energy deposits in the CAL cells and in the MC it was also applied to the final-state hadrons. The jet search was performed in the $\eta - \phi$ plane of the laboratory, starting with the CAL cells or hadrons as initial objects. In the following discussion, $E_{T,i}$ denotes the transverse energy, η_i the pseudorapidity and ϕ_i the azimuthal angle of object i in the laboratory frame. For each pair of objects, the quantity

$$d_{ij} = [(\eta_i - \eta_j)^2 + (\phi_i - \phi_j)^2] \cdot \min(E_{T,i}, E_{T,j})^2$$

was calculated. For each individual object, the quantity $d_i = (E_{T,i})^2$ was also calculated. If, of all the values $\{d_{ij}, d_i\}$, d_{kl} was the smallest, then objects k and l were combined into a single new object. If, however, d_k was the smallest, then object k was considered a jet and was excluded from further clustering. The procedure was repeated until all objects were assigned to jets. The jet variables were defined according to the Snowmass convention [33]:

$$E_T^{\rm jet} = \sum_i E_{T,i}, \eta^{\rm jet} = \sum_i \frac{E_{T,i}\eta_i}{E_T^{\rm jet}}, \phi^{\rm jet} = \sum_i \frac{E_{T,i}\phi_i}{E_T^{\rm jet}},$$

where the sums run over all objects associated with the given jet. This prescription was also used to determine these variables for the subjets. For jets constructed from CAL cells, jet energies were corrected for all energy-loss effects, principally in inactive material of typically about one radiation length, in front of the CAL (see Sect. 4).

For the inclusive jet sample, all jets with $E_T^{\rm jet} > 14$ GeV and $-1 < \eta^{\rm jet} < 2$ were retained. For the dijet sample, at least one additional jet with $E_T^{\rm jet} > 5$ GeV and $-1 < \eta^{\rm jet} < 2$ was required. The upper rapidity requirement is made so that the jet is within the CTD acceptance for efficient background rejection. There are very few events with jets with sufficient $E_T^{\rm jet}$ below the lower rapidity requirement.

With the above criteria, 1865 events with at least one jet and 282 dijet events were identified.

3.1 Definition of subjet multiplicity

Subjets were resolved within a jet by considering all objects associated with the jet and by repeating the application of the k_T cluster algorithm described above, until for every pair of objects i and j, the quantity d_{ij} was greater than $d_{\rm cut} = y_{\rm cut} \cdot \left(E_T^{\rm jet}\right)^2$. All remaining objects were called subjets. The jet structure depends upon the value chosen for the resolution parameter $y_{\rm cut}$. For each sample studied, the mean subjet multiplicity, $\langle n_{\rm sbj} \rangle$, is defined as the average number of subjets contained in a jet at a given value of $y_{\rm cut}$:

$$\langle n_{\rm sbj}(y_{\rm cut}) \rangle = \frac{1}{N_{\rm jets}} \sum_{i=1}^{N_{\rm jets}} n_{\rm sbj}^i(y_{\rm cut}),$$

where $n_{\rm sbj}^i$ is the number of subjets in jet i and $N_{\rm jets}$ is the total number of jets in the sample. The mean subjet multiplicity of the inclusive jet sample was measured for $y_{\rm cut}$ values in the range $5 \cdot 10^{-4}$ to 0.1. The $y_{\rm cut}$ range was chosen to be small enough to have mean subjet multiplicities larger than unity and large enough to avoid the degradation in resolution caused by the finite size of the CAL cells.

4 Monte Carlo simulation

Samples of events were generated to determine the response of the detector to jets of hadrons and to evaluate the correction factors necessary to obtain the hadron-level jet cross sections and subjet multiplicities. The CC DIS events were generated using the LEPTO 6.5 program [34] interfaced to HERACLES 4.6.1 [35, 36] via DJANGOH 1.1 [37,38]. The HERACLES program includes first-order electroweak radiative corrections. The CTEQ4D [39] NLO proton parton distribution functions (PDF) were used. The QCD radiation was modelled with the colour-dipole model [40–43] by using the ARIADNE 4.08 program [44,45] including the boson-gluon-fusion process. As an alternative, samples of events were generated using the LEPTO model which is based on first-order QCD matrix elements and parton showers. For the generation of the LEPTO samples, the option for soft-colour interactions was switched off since its inclusion results in an increase both in particle multiplicity and energy per unit of rapidity that disagrees with the measurements in NC DIS at HERA [46]. In both cases, fragmentation into hadrons was performed using the Lund string model [47] as implemented in JETSET 7.4 [48, 49]. To calculate the acceptances and to estimate hadronisation effects, the generated events were passed through the GEANT 3.13-based [50] simulation of the ZEUS detector and trigger. They were reconstructed and analysed by the same program chain as used for data. For both the ARIADNE and LEPTO event samples, a good description of the measured distributions for the kinematic and jet variables was obtained [51].

To correct the data to hadron level, multiplicative correction factors, defined as the ratio of the measured quantities for jets of hadrons over the same quantity for jets at detector level, were estimated by using the ARIADNE and LEPTO models. Parton-level predictions were also obtained by applying the jet algorithm to the MC-generated

partons. These predictions were used to correct the NLO QCD calculations to hadron level (Sect. 5).

HERACLES 4.6.2 [35,36] was used to correct the measured cross sections to the electroweak Born level evaluated using the electromagnetic coupling constant $\alpha = 1/137.03599$, the Fermi coupling constant $G_F = 1.16639 \cdot 10^{-5}\ GeV^{-2}$ and the mass of the Z boson $M_Z = 91.1882$ GeV [60] to determine the electroweak parameters.

5 NLO QCD calculations

The NLO QCD calculations were obtained from the program MEPJET [52], which employs the phase-space slicing method [53]. This is the only available program providing NLO calculations for jet production in charged current deep inelastic scattering. The calculations were performed in the $\overline{MS}$ renormalisation and factorisation schemes. The number of flavours was set to five and the renormalisation (μ_R) and factorisation (μ_F) scales were chosen to be $\mu_R = \mu_F = Q$. The calculations were performed using the CTEQ4M [39] parametrisations of the proton PDFs, which are based on the $\overline{MS}$ scheme. The jet algorithm described in Sect. 3 was also applied to the partons in the events generated by MEPJET in order to compute the jet cross section and the predictions for the subjet multiplicities. The cross sections were evaluated using the same values for α, G_F and M_Z as in the electroweak Born level of the measured cross sections (Sect. 4). In addition, the mass of the W boson was fixed to 80.4603 GeV.

Since the measurements correspond to jets of hadrons whereas the NLO QCD calculations correspond to jet of partons, the predictions were corrected to the hadron level using the MC simulations. The multiplicative correction factor ($C_{\rm had}$) is defined as the ratio of either the cross sections or the mean subjet multiplicities for jets of hadrons to the same quantity for jets of partons, estimated using the MC programs described in Sect. 4. The ratios obtained with the ARIADNE and LEPTO models were in good agreement and the mean was taken as the value of $C_{\rm had}$. The value of $C_{\rm had}$ is $\sim$ 1.03 ($\sim$ 1.10) for the inclusive jet (dijet) cross sections. For the mean subjet multiplicity, $C_{\rm had}$ is 2.13 at $y_{\rm cut} = 5 \cdot 10^{-4}$ and $14 < E_T^{\rm jet} < 17$ GeV and approaches unity as $y_{\rm cut}$ and $E_T^{\rm jet}$ increase.

The theoretical predictions were redetermined after changing the parameters as described below. In each case the difference between the redetermination and the nominal prediction was taken to be the uncertainty in the calculation associated with the parameter under consideration.

- Proton PDFs: the CTEQ5M [54] and MRST [55, 56] sets, rather than CTEQ4M [39] , were used. Also, a set of the MRST PDFs with a larger d/u quark ratio at large Bjorken x was used. The uncertainty in the cross sections was less than $\sim$ 4% for the inclusive jet cross section, except for high $E_T^{\rm jet}$, where it reaches $\sim$ 20%. It was less than $\sim$ 10% for the dijet cross sections. The uncertainty was negligible for the subjet multiplicities;
- $\alpha_s(M_Z)$: the $\alpha_s(M_Z)$ values of 0.113 and 0.119, corresponding to the proton PDFs CTEQ4A2 and CTEQ4A4, were used. The uncertainty in the cross sections was typically $\sim$ 2%; for the mean subjet multiplicity the uncertainty was $\sim$ 1% ;
- μ_R: in order to estimate the effects of the terms beyond NLO, the scale μ_R was varied between $Q/2$ and $2Q$, while keeping μ_F fixed at Q. The uncertainty of the cross sections was less than 5%. The uncertainty on the mean subjet multiplicity was $\sim$ 3% for $y_{\rm cut} = 10^{-2}$;
- $C_{\rm had}$: the hadronisation correction, $C_{\rm had}$, was varied by half of the difference between those evaluated using ARIADNE and LEPTO. The uncertainty typically amounted to less than 1%(3%) for inclusive jet (dijet) cross sections. For the subjet multiplicities, the uncertainty was less than 3% for $y_{\rm cut} = 10^{-2}$.
- $s_{\rm min}$: the cut-off parameter $s_{\rm min}$ in the phase-space slicing was changed from the default value of 0.1 GeV^2 to 0.01 GeV^2. This uncertainty was less than 1% in all the calculations and was neglected in the estimation of the total theoretical uncertainty.

The total theoretical uncertainty was obtained by adding in quadrature the individual uncertainties listed above and is shown as the hatched band in the figures.

6 Experimental systematic uncertainties

A study of the sources contributing to the systematic uncertainties of the measurements was carried out. The following sources were considered:

- the uncertainty on the absolute energy scale of the jets was taken to be $\pm$1% for $E_T^{\rm jet} > 10$ GeV and $\pm$3% for lower $E_T^{\rm jet}$ values [57–59]. The resulting uncertainty was less than 5% (12 %) for the inclusive jet (dijet) cross sections and less than 2% for the mean subjet multiplicity;
- the uncertainty in the reconstruction of the kinematic variables due to that in the absolute energy scale of the CAL was estimated by varying the energy variables measured with the CAL by $\pm$3%. The uncertainty was less than 5% for all distributions;
- the differences in the results obtained by using ARIADNE or LEPTO to correct the data for detector effects were taken as systematic uncertainties; they were typically smaller than 5% for the cross sections and smaller than 2% for the mean subjet multiplicities;
- the selection cut of $\not{p}_T > 11$ GeV was changed to 10 GeV and 12 GeV. This gave a variation of the cross sections (subjet multiplicities) of less than 5% (2%). The uncertainty evaluated from the variation of other selection cuts was typically less than 2%.

For the jet cross sections, the systematic uncertainties not associated with the absolute energy scale of the jets and the CAL are not point-to-point correlated and were added in quadrature to the statistical errors. They are shown as the bars in the figures. The uncertainty due to the absolute energy scale is point-to-point correlated and is shown separately as a shaded band in each figure. For the

Table 1. Inclusive jet cross-section $d\sigma/dQ^2$ for jets of hadrons in the laboratory frame. The statistical, systematic and energy-scale uncertainties are shown separately. The multiplicative correction applied to correct for QED radiative effects and for hadronisation effects and the theoretical correction factor used to combine the two data sets are shown

1995–1997 e^+p data sample ($\sqrt{s} = 300$ GeV)						
Q^2 range (GeV^2)	$d\sigma/dQ^2$ ($\mathrm{pb/GeV}^2$)	Δ_{stat}	Δ_{syst}	Δ_{ES}	QED correction	C_{had}
200–500	0.0105	± 0.0010	$^{+0.0012}_{-0.0010}$	$^{+0.0014}_{-0.0011}$	1.045	0.985
500–1000	0.0108	± 0.0008	$^{+0.0007}_{-0.0005}$	$^{+0.0004}_{-0.0004}$	1.033	1.000
1000–2000	0.00571	± 0.00042	$^{+0.00014}_{-0.00037}$	$^{+0.00006}_{-0.00003}$	1.042	1.001
2000–4000	0.00221	± 0.00018	$^{+0.00005}_{-0.00008}$	$^{+0.00007}_{-0.00004}$	1.064	0.999
4000–10000	0.000380	$\pm 4.1 \cdot 10^{-5}$	$^{+1.0}_{-1.1} \cdot 10^{-5}$	$^{+3.6}_{-3.0} \cdot 10^{-5}$	1.085	0.998
1999–2000 e^+p data sample ($\sqrt{s} = 318$ GeV)						
Q^2 range (GeV^2)	$d\sigma/dQ^2$ ($\mathrm{pb/GeV}^2$)	Δ_{stat}	Δ_{syst}	Δ_{ES}	QED correction	C_{had}
200–500	0.0125	± 0.0010	$^{+0.0012}_{-0.0014}$	$^{+0.0016}_{-0.0013}$	1.055	0.983
500–1000	0.0107	± 0.0007	$^{+0.0007}_{-0.0006}$	$^{+0.0005}_{-0.0005}$	1.048	0.999
1000–2000	0.00668	± 0.00038	$^{+0.00010}_{-0.00014}$	$^{+0.00009}_{-0.00007}$	1.054	1.000
2000–4000	0.00233	± 0.00016	$^{+0.00002}_{-0.00008}$	$^{+0.00006}_{-0.00004}$	1.073	0.998
4000–10000	0.000489	$\pm 4.0 \cdot 10^{-5}$	$^{+0.9}_{-1.3} \cdot 10^{-5}$	$^{+4.3}_{-3.3} \cdot 10^{-5}$	1.097	0.997
Combined 1995–2000 e^+p data sample ($\sqrt{s} = 318$ GeV)						
Q^2 range (GeV^2)	$d\sigma/dQ^2$ ($\mathrm{pb/GeV}^2$)	Δ_{stat}	Δ_{syst}	Δ_{ES}	$\sigma^{th}_{318}/\sigma^{th}_{300}$	
200–500	0.0119	± 0.0007	$^{+0.0012}_{-0.0012}$	$^{+0.0016}_{-0.0013}$	1.0476	
500–1000	0.0110	± 0.0005	$^{+0.0007}_{-0.0005}$	$^{+0.0005}_{-0.0004}$	1.0580	
1000–2000	0.00647	± 0.00029	$^{+0.00008}_{-0.00018}$	$^{+0.00008}_{-0.00005}$	1.0750	
2000–4000	0.00237	± 0.00012	$^{+0.00002}_{-0.00007}$	$^{+0.00007}_{-0.00005}$	1.1022	
4000–10000	0.000472	$\pm 3.1 \cdot 10^{-5}$	$^{+0.7}_{-1.2} \cdot 10^{-5}$	$^{+4.2}_{-3.4} \cdot 10^{-5}$	1.1633	

Table 2. Inclusive jet cross-section $d\sigma/d\eta^{\mathrm{jet}}$ for jets of hadrons in the laboratory frame. For details, see the caption to Table 1

1995–1997 e^+p data sample ($\sqrt{s} = 300$ GeV)						
η^{jet} range	$d\sigma/d\eta^{\mathrm{jet}}$ (pb)	Δ_{stat}	Δ_{syst}	Δ_{ES}	QED correction	C_{had}
-1 to 0	3.80	± 0.37	$^{+0.25}_{-0.31}$	$^{+0.14}_{-0.10}$	1.082	0.967
0 to 1	9.60	± 0.53	$^{+0.37}_{-0.51}$	$^{+0.05}_{-0.05}$	1.052	0.992
1 to 1.5	10.53	± 0.79	$^{+0.22}_{-0.38}$	$^{+0.05}_{-0.04}$	1.045	1.005
1.5 to 2	7.78	± 0.67	$^{+0.55}_{-0.40}$	$^{+0.04}_{-0.02}$	1.042	1.017
1999–2000 e^+p data sample ($\sqrt{s} = 318$ GeV)						
η^{jet} range	$d\sigma/d\eta^{\mathrm{jet}}$ (pb)	Δ_{stat}	Δ_{syst}	Δ_{ES}	QED correction	C_{had}
-1 to 0	4.76	± 0.35	$^{+0.11}_{-0.44}$	$^{+0.20}_{-0.15}$	1.086	0.967
0 to 1	9.73	± 0.45	$^{+0.38}_{-0.23}$	$^{+0.06}_{-0.04}$	1.064	0.991
1 to 1.5	11.46	± 0.69	$^{+0.19}_{-0.16}$	$^{+0.06}_{-0.04}$	1.058	1.003
1.5 to 2	9.55	± 0.62	$^{+0.25}_{-0.29}$	$^{+0.04}_{-0.04}$	1.060	1.013
Combined 1995–2000 e^+p data sample ($\sqrt{s} = 318$ GeV)						
η^{jet} range	$d\sigma/d\eta^{\mathrm{jet}}$ (pb)	Δ_{stat}	Δ_{syst}	Δ_{ES}	$\sigma^{th}_{318}/\sigma^{th}_{300}$	
-1 to 0	4.48	± 0.26	$^{+0.16}_{-0.39}$	$^{+0.18}_{-0.13}$	1.0670	
0 to 1	9.98	± 0.35	$^{+0.38}_{-0.31}$	$^{+0.06}_{-0.05}$	1.0797	
1 to 1.5	11.50	± 0.54	$^{+0.17}_{-0.19}$	$^{+0.06}_{-0.04}$	1.0990	
1.5 to 2	9.26	± 0.48	$^{+0.32}_{-0.31}$	$^{+0.04}_{-0.03}$	1.1299	

Table 3. Inclusive jet cross-section $d\sigma/dE_T^{\rm jet}$ for jets of hadrons in the laboratory frame. For details, see the caption to Table 1

1995–1997 e^+p data sample ($\sqrt{s} = 300$ GeV)						
$E_T^{\rm jet}$ range (GeV)	$d\sigma/dE_T^{\rm jet}$ (pb/GeV)	$\Delta_{\rm stat}$	$\Delta_{\rm syst}$	$\Delta_{\rm ES}$	QED correction	$C_{\rm had}$
14–21	0.950	±0.068	$^{+0.081}_{-0.069}$	$^{+0.014}_{-0.014}$	1.025	0.992
21–29	0.703	±0.052	$^{+0.040}_{-0.051}$	$^{+0.006}_{-0.004}$	1.036	0.998
29–41	0.486	±0.034	$^{+0.008}_{-0.022}$	$^{+0.006}_{-0.004}$	1.066	0.998
41–55	0.219	±0.021	$^{+0.008}_{-0.007}$	$^{+0.004}_{-0.004}$	1.094	0.998
55–71	0.0542	±0.0096	$^{+0.0026}_{-0.0026}$	$^{+0.0020}_{-0.0020}$	1.131	0.988
71–87	0.0210	±0.0058	$^{+0.0007}_{-0.0008}$	$^{+0.0011}_{-0.0012}$	1.147	0.986
87–119	0.00643	±0.00214	$^{+0.00121}_{-0.00064}$	$^{+0.00070}_{-0.00047}$	1.219	0.981
1999–2000 e^+p data sample ($\sqrt{s} = 318$ GeV)						
$E_T^{\rm jet}$ range (GeV)	$d\sigma/dE_T^{\rm jet}$ (pb/GeV)	$\Delta_{\rm stat}$	$\Delta_{\rm syst}$	$\Delta_{\rm ES}$	QED correction	$C_{\rm had}$
14–21	1.030	±0.060	$^{+0.056}_{-0.092}$	$^{+0.014}_{-0.012}$	1.035	0.989
21–29	0.816	±0.047	$^{+0.022}_{-0.034}$	$^{+0.008}_{-0.007}$	1.052	0.995
29–41	0.527	±0.030	$^{+0.014}_{-0.007}$	$^{+0.006}_{-0.005}$	1.071	0.998
41–55	0.230	±0.018	$^{+0.003}_{-0.006}$	$^{+0.004}_{-0.004}$	1.112	0.998
55–71	0.0775	±0.0096	$^{+0.0026}_{-0.0035}$	$^{+0.0026}_{-0.0026}$	1.135	0.990
71–87	0.0232	±0.0052	$^{+0.0010}_{-0.0012}$	$^{+0.0012}_{-0.0012}$	1.172	0.986
87–119	0.00385	±0.00146	$^{+0.00034}_{-0.00012}$	$^{+0.00036}_{-0.00033}$	1.192	0.984
Combined 1995–2000 e^+p data sample ($\sqrt{s} = 318$ GeV)						
$E_T^{\rm jet}$ range (GeV)	$d\sigma/dE_T^{\rm jet}$ (pb/GeV)	$\Delta_{\rm stat}$	$\Delta_{\rm syst}$	$\Delta_{\rm ES}$	$\sigma^{th}_{318}/\sigma^{th}_{300}$	
14–21	1.022	±0.046	$^{+0.067}_{-0.084}$	$^{+0.014}_{-0.013}$	1.0621	
21–29	0.791	±0.036	$^{+0.027}_{-0.034}$	$^{+0.007}_{-0.006}$	1.0688	
29–41	0.527	±0.023	$^{+0.009}_{-0.009}$	$^{+0.006}_{-0.005}$	1.0855	
41–55	0.236	±0.014	$^{+0.004}_{-0.004}$	$^{+0.004}_{-0.004}$	1.1216	
55–71	0.0727	±0.0074	$^{+0.0020}_{-0.0029}$	$^{+0.0025}_{-0.0025}$	1.1891	
71–87	0.0246	±0.0043	$^{+0.0010}_{-0.0008}$	$^{+0.0013}_{-0.0014}$	1.3046	
87–119	0.00572	±0.00143	$^{+0.00066}_{-0.00027}$	$^{+0.00058}_{-0.00045}$	1.5461	

subjet multiplicities all the systematic uncertainties are point-to-point correlated and were added in quadrature to the statistical errors. They are shown as the bars in the figures.

In addition, there is an overall normalisation uncertainty of 2.0% from the luminosity determination, which is not included in the results presented in the figures and the tables of the cross sections.

7 Results

7.1 Data-combination method

Due to the different centre-of-mass energy of the two data sets used in the analysis, the measured jet cross sections based on each set are presented separately in Tables 1 to 5.

The measured jet cross sections, $\sigma_{\sqrt{s}}$, were combined using the following formula:

$$\sigma^{\rm comb}_{318} = \frac{\sigma_{300}\cdot\mathcal{L}_{300} + \sigma_{318}\cdot\mathcal{L}_{318}}{\mathcal{L}_{300}\cdot(\sigma^{th}_{300}/\sigma^{th}_{318}) + \mathcal{L}_{318}},$$

where $\mathcal{L}_{\sqrt{s}}$ is the luminosity and $\sigma^{th}_{\sqrt{s}}$ is the predicted cross section. The ratio $\sigma^{th}_{300}/\sigma^{th}_{318}$ was obtained using the program MEPJET. The ratio obtained by ARIADNE is within 1% of that obtained by MEPJET and was the same, within statistical errors, as that measured in the data. All the systematic errors have been assumed to be correlated between the measurements.

No dependence of the subjet multiplicities with the centre-of-mass energy was seen either in the data or in the theoretical predictions; thus the subjet multiplicities were calculated using the inclusive jet sample of both data sets. The measured subjet multiplicities are presented in Tables 6 to 9.

7.2 Inclusive jet differential cross sections

The differential inclusive jet cross sections were measured in the kinematic region defined by $Q^2 > 200$ GeV^2 and $y < 0.9$. These cross sections include every jet of hadrons in the event with $E_T^{\rm jet} > 14$ GeV and $-1 < \eta^{\rm jet} < 2$. The

Table 4. Dijet cross-section $d\sigma/dQ^2$ for jets of hadrons in the laboratory frame. For details, see the caption to Table 1

1995–1997 e^+p data sample ($\sqrt{s} = 300$ GeV)						
Q^2 range (GeV^2)	$d\sigma/dQ^2$ (pb/GeV^2)	$\Delta_{\rm stat}$	$\Delta_{\rm syst}$	$\Delta_{\rm ES}$	QED correction	$C_{\rm had}$
200–500	0.00153	± 0.00051	$^{+0.00030}_{-0.00067}$	$^{+0.00031}_{-0.00023}$	1.040	0.916
500–1000	0.00165	± 0.00034	$^{+0.00015}_{-0.00022}$	$^{+0.00014}_{-0.00013}$	1.045	0.924
1000–2000	0.00112	± 0.00020	$^{+0.00006}_{-0.00007}$	$^{+0.00003}_{-0.00003}$	1.059	0.926
2000–4000	$3.85 \cdot 10^{-4}$	$\pm 0.82 \cdot 10^{-4}$	$^{+0.25}_{-0.26} \cdot 10^{-4}$	$^{+0.26}_{-0.15} \cdot 10^{-4}$	1.077	0.910
4000–10000	$7.13 \cdot 10^{-5}$	$\pm 1.91 \cdot 10^{-5}$	$^{+0.70}_{-0.12} \cdot 10^{-5}$	$^{+0.77}_{-0.79} \cdot 10^{-5}$	1.083	0.893
1999–2000 e^+p data sample ($\sqrt{s} = 318$ GeV)						
Q^2 range (GeV^2)	$d\sigma/dQ^2$ (pb/GeV^2)	$\Delta_{\rm stat}$	$\Delta_{\rm syst}$	$\Delta_{\rm ES}$	QED correction	$C_{\rm had}$
200–500	0.00290	± 0.00062	$^{+0.00081}_{-0.00079}$	$^{+0.00057}_{-0.00043}$	1.068	0.914
500–1000	0.00190	± 0.00031	$^{+0.00023}_{-0.00026}$	$^{+0.00017}_{-0.00015}$	1.054	0.925
1000–2000	0.00112	± 0.00016	$^{+0.00006}_{-0.00007}$	$^{+0.00004}_{-0.00003}$	1.067	0.927
2000–4000	$4.02 \cdot 10^{-4}$	$\pm 0.70 \cdot 10^{-4}$	$^{+0.27}_{-0.32} \cdot 10^{-4}$	$^{+0.16}_{-0.15} \cdot 10^{-4}$	1.078	0.916
4000–10000	$11.70 \cdot 10^{-5}$	$\pm 2.04 \cdot 10^{-5}$	$^{+1.12}_{-0.99} \cdot 10^{-5}$	$^{+1.32}_{-0.99} \cdot 10^{-5}$	1.101	0.904
Combined 1995–2000 e^+p data sample ($\sqrt{s} = 318$ GeV)						
Q^2 range (GeV^2)	$d\sigma/dQ^2$ (pb/GeV^2)	$\Delta_{\rm stat}$	$\Delta_{\rm syst}$	$\Delta_{\rm ES}$	$\sigma^{th}_{318}/\sigma^{th}_{300}$	
200–500	0.00242	± 0.00043	$^{+0.00050}_{-0.00069}$	$^{+0.00048}_{-0.00036}$	1.0848	
500–1000	0.00186	± 0.00024	$^{+0.00019}_{-0.00024}$	$^{+0.00016}_{-0.00015}$	1.0859	
1000–2000	0.00116	± 0.00013	$^{+0.00006}_{-0.00005}$	$^{+0.00004}_{-0.00003}$	1.0926	
2000–4000	$4.13 \cdot 10^{-4}$	$\pm 0.56 \cdot 10^{-4}$	$^{+0.25}_{-0.28} \cdot 10^{-4}$	$^{+0.21}_{-0.16} \cdot 10^{-4}$	1.1191	
4000–10000	$10.49 \cdot 10^{-5}$	$\pm 1.53 \cdot 10^{-5}$	$^{+0.98}_{-0.57} \cdot 10^{-5}$	$^{+1.17}_{-0.97} \cdot 10^{-5}$	1.1777	

Table 5. Dijet cross-section $d\sigma/dm_{12}$ for jets of hadrons in the laboratory frame. For details, see the caption to Table 1

1995–1997 e^+p data sample ($\sqrt{s} = 300$ GeV)						
m_{12} range (GeV)	$d\sigma/dm_{12}$ (pb/GeV)	$\Delta_{\rm stat}$	$\Delta_{\rm syst}$	$\Delta_{\rm ES}$	QED correction	$C_{\rm had}$
10–20	0.0724	± 0.0137	$^{+0.0030}_{-0.0084}$	$^{+0.0019}_{-0.0011}$	1.050	0.921
20–30	0.104	± 0.018	$^{+0.006}_{-0.007}$	$^{+0.002}_{-0.003}$	1.053	0.901
30–40	0.0884	± 0.0184	$^{+0.0098}_{-0.0092}$	$^{+0.0038}_{-0.0029}$	1.060	0.918
40–75	0.0296	± 0.0068	$^{+0.0054}_{-0.0046}$	$^{+0.0015}_{-0.0014}$	1.089	0.942
1999–2000 e^+p data sample ($\sqrt{s} = 318$ GeV)						
m_{12} range (GeV)	$d\sigma/dm_{12}$ (pb/GeV)	$\Delta_{\rm stat}$	$\Delta_{\rm syst}$	$\Delta_{\rm ES}$	QED correction	$C_{\rm had}$
10–20	0.0913	± 0.0129	$^{+0.0094}_{-0.0045}$	$^{+0.0016}_{-0.0019}$	1.059	0.918
20–30	0.140	± 0.018	$^{+0.008}_{-0.011}$	$^{+0.004}_{-0.003}$	1.064	0.902
30–40	0.110	± 0.018	$^{+0.010}_{-0.009}$	$^{+0.005}_{-0.004}$	1.082	0.917
40–75	0.0228	± 0.0049	$^{+0.0045}_{-0.0021}$	$^{+0.0010}_{-0.0011}$	1.085	0.941
Combined 1995–2000 e^+p data sample ($\sqrt{s} = 318$ GeV)						
m_{12} range (GeV)	$d\sigma/dm_{12}$ (pb/GeV)	$\Delta_{\rm stat}$	$\Delta_{\rm syst}$	$\Delta_{\rm ES}$	$\sigma^{th}_{318}/\sigma^{th}_{300}$	
10–20	0.0863	± 0.0098	$^{+0.0058}_{-0.0057}$	$^{+0.0018}_{-0.0016}$	1.0830	
20–30	0.130	± 0.013	$^{+0.006}_{-0.009}$	$^{+0.003}_{-0.003}$	1.0992	
30–40	0.106	± 0.013	$^{+0.009}_{-0.008}$	$^{+0.005}_{-0.003}$	1.1172	
40–75	0.0270	± 0.0042	$^{+0.0051}_{-0.0031}$	$^{+0.0013}_{-0.0013}$	1.1552	

Table 6. Mean subjet multiplicity as a function of $y_{\rm cut}$ for the $E_T^{\rm jet}$ regions $14 < E_T^{\rm jet} < 17$ and $17 < E_T^{\rm jet} < 21$ GeV. The statistical and systematic uncertainties are shown separately. The multiplicative correction applied to correct for hadronisation effects is shown in the last column

y_{cut} value	$\langle n_{\rm sbj}\rangle$	$\Delta_{\rm stat}$	$\Delta_{\rm syst}$	$C_{\rm had}$
$14 < E_T^{\rm jet} < 17$ GeV				
0.0005	4.432	±0.082	$^{+0.078}_{-0.025}$	2.127
0.001	3.576	±0.071	$^{+0.098}_{-0.020}$	1.845
0.003	2.616	±0.057	$^{+0.058}_{-0.020}$	1.526
0.005	2.238	±0.050	$^{+0.039}_{-0.022}$	1.426
0.01	1.755	±0.042	$^{+0.026}_{-0.031}$	1.292
0.03	1.263	±0.033	$^{+0.028}_{-0.015}$	1.094
0.05	1.117	±0.023	$^{+0.019}_{-0.013}$	1.037
0.1	1.010	±0.007	$^{+0.018}_{-0.003}$	1.005
$17 < E_T^{\rm jet} < 21$ GeV				
0.0005	4.272	±0.071	$^{+0.067}_{-0.050}$	1.989
0.001	3.522	±0.060	$^{+0.058}_{-0.043}$	1.726
0.003	2.427	±0.047	$^{+0.049}_{-0.025}$	1.464
0.005	1.999	±0.042	$^{+0.036}_{-0.012}$	1.364
0.01	1.574	±0.034	$^{+0.021}_{-0.017}$	1.227
0.03	1.176	±0.026	$^{+0.014}_{-0.018}$	1.054
0.05	1.102	±0.020	$^{+0.021}_{-0.010}$	1.016
0.1	1.021	±0.009	$^{+0.006}_{-0.006}$	0.999

Table 7. Mean subjet multiplicity as a function of $y_{\rm cut}$ for the $E_T^{\rm jet}$ regions $21 < E_T^{\rm jet} < 25$ and $25 < E_T^{\rm jet} < 35$ GeV. For details, see the caption to Table 6

y_{cut} value	$\langle n_{\rm sbj}\rangle$	$\Delta_{\rm stat}$	$\Delta_{\rm syst}$	$C_{\rm had}$
$21 < E_T^{\rm jet} < 25$ GeV				
0.0005	4.051	±0.070	$^{+0.067}_{-0.010}$	1.857
0.001	3.251	±0.059	$^{+0.071}_{-0.011}$	1.637
0.003	2.266	±0.043	$^{+0.052}_{-0.014}$	1.409
0.005	1.953	±0.038	$^{+0.042}_{-0.008}$	1.304
0.01	1.504	±0.034	$^{+0.035}_{-0.007}$	1.167
0.03	1.164	±0.025	$^{+0.023}_{-0.008}$	1.025
0.05	1.070	±0.017	$^{+0.023}_{-0.005}$	1.003
0.1	1.022	±0.009	$^{+0.008}_{-0.005}$	0.997
$25 < E_T^{\rm jet} < 35$ GeV				
0.0005	3.786	±0.049	$^{+0.027}_{-0.021}$	1.736
0.001	2.997	±0.039	$^{+0.028}_{-0.011}$	1.570
0.003	2.067	±0.029	$^{+0.017}_{-0.009}$	1.339
0.005	1.717	±0.025	$^{+0.019}_{-0.012}$	1.228
0.01	1.386	±0.023	$^{+0.018}_{-0.009}$	1.099
0.03	1.137	±0.016	$^{+0.005}_{-0.012}$	1.006
0.05	1.061	±0.011	$^{+0.003}_{-0.013}$	0.998
0.1	1.008	±0.004	$^{+0.004}_{-0.004}$	0.998

Table 8. Mean subjet multiplicity as a function of $y_{\rm cut}$ for the $E_T^{\rm jet}$ regions $35 < E_T^{\rm jet} < 55$ and $55 < E_T^{\rm jet} < 119$ GeV. For details, see the caption to Table 6

y_{cut} value	$\langle n_{\rm sbj}\rangle$	$\Delta_{\rm stat}$	$\Delta_{\rm syst}$	$C_{\rm had}$
$35 < E_T^{\rm jet} < 55$ GeV				
0.0005	3.343	±0.045	$^{+0.037}_{-0.017}$	1.579
0.001	2.649	±0.040	$^{+0.038}_{-0.013}$	1.433
0.003	1.797	±0.029	$^{+0.029}_{-0.009}$	1.197
0.005	1.512	±0.026	$^{+0.027}_{-0.006}$	1.106
0.01	1.245	±0.022	$^{+0.020}_{-0.004}$	1.026
0.03	1.106	±0.015	$^{+0.003}_{-0.002}$	0.996
0.05	1.060	±0.011	$^{+0.005}_{-0.001}$	0.996
0.1	1.010	±0.004	$^{+0.001}_{-0.000}$	0.998
$55 < E_T^{\rm jet} < 119$ GeV				
0.0005	2.790	±0.068	$^{+0.013}_{-0.035}$	1.450
0.001	2.196	±0.056	$^{+0.022}_{-0.026}$	1.285
0.003	1.520	±0.041	$^{+0.038}_{-0.012}$	1.073
0.005	1.378	±0.042	$^{+0.040}_{-0.015}$	1.022
0.01	1.260	±0.039	$^{+0.024}_{-0.012}$	0.998
0.03	1.098	±0.025	$^{+0.005}_{-0.007}$	0.996
0.05	1.044	±0.017	$^{+0.005}_{-0.003}$	0.998
0.1	1.036	±0.026	$^{+0.004}_{-0.002}$	1.000

Table 9. Measurement of the mean subjet multiplicity at $y_{\rm cut} = 10^{-2}$ as a function of Q^2. For details, see the caption to Table 6

Q^2 range (GeV^2)	$\langle n_{\rm sbj}\rangle$	$\Delta_{\rm stat}$	$\Delta_{\rm syst}$	$C_{\rm had}$
200–350	1.695	±0.053	$^{+0.025}_{-0.027}$	1.316
350–500	1.677	±0.050	$^{+0.011}_{-0.049}$	1.257
500–750	1.516	±0.036	$^{+0.028}_{-0.011}$	1.212
750–1000	1.487	±0.040	$^{+0.042}_{-0.018}$	1.175
1000–2000	1.391	±0.024	$^{+0.030}_{-0.012}$	1.129
2000–4000	1.372	±0.027	$^{+0.012}_{-0.014}$	1.081
4000–10000	1.318	±0.031	$^{+0.034}_{-0.010}$	1.051

differential inclusive jet cross sections as a function of Q^2, $\eta^{\rm jet}$ and $E_T^{\rm jet}$ are shown in Figs. 1 to 3. Both the ARIADNE MC model and the NLO QCD calculation MEPJET give a good description of the measured inclusive jet cross sections.

7.3 Dijet differential cross sections

The differential dijet cross sections were measured in the kinematic region defined by $Q^2 > 200$ GeV^2 and $y < 0.9$. These cross sections refer to the two jets of hadrons with highest transverse energy in the event with $E_T^{\rm jet,1} >$

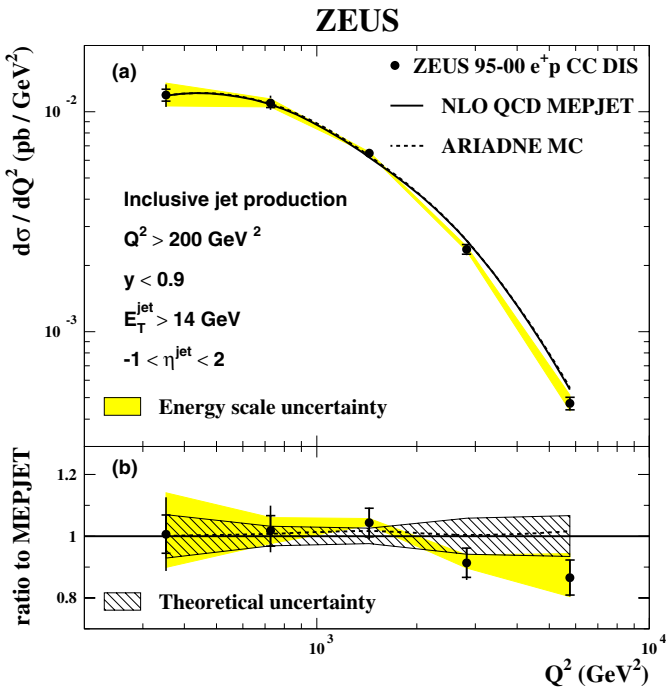

Fig. 1. a The differential cross-section $d\sigma/dQ^2$ for inclusive jet production in the laboratory frame with $E_T^{jet} > 14$ GeV and $-1 < \eta^{jet} < 2$ in the kinematic region $Q^2 > 200$ GeV ^{2} and $y < 0.9$ for the 1995-2000 e^+p data (black dots). The data are corrected to hadron level. The inner error bars represent the statistical uncertainty of the data, the outer error bars show the statistical and the systematic uncertainties (not associated with the uncertainty in the absolute energy scale) added in quadrature. The shaded band displays the uncertainty due to the absolute energy scale of the CAL. The parton shower Monte Carlo prediction given by ARIADNE at hadron level (dashed line) and the next-to-leading-order prediction obtained with MEPJET corrected to hadron level (solid line) are shown. **b** The ratio of the measured cross section to the next-to-leading-order calculation. The theoretical uncertainty is indicated by the hatched band

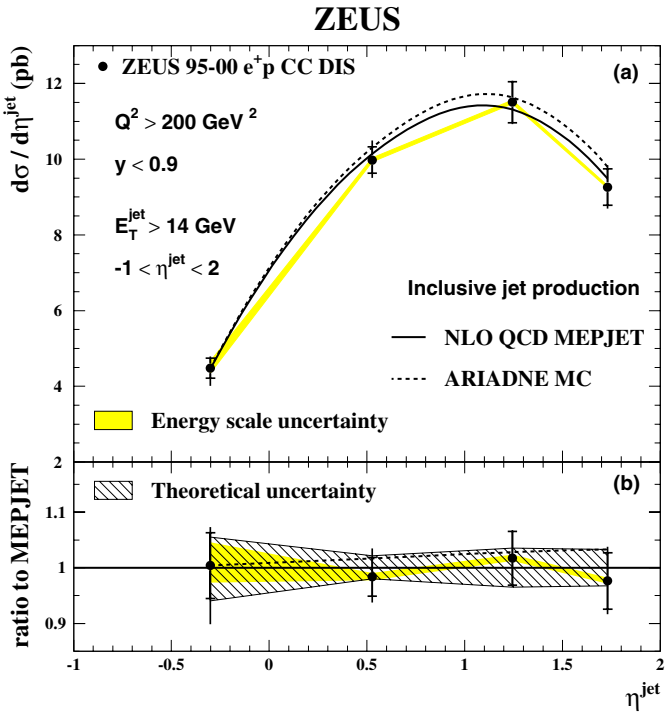

Fig. 2. a The differential cross-section $d\sigma/d\eta^{jet}$ for inclusive jet production in the laboratory frame with $E_T^{jet} > 14$ GeV and $-1 < \eta^{jet} < 2$ in the kinematic region $Q^2 > 200$ GeV ^{2} and $y < 0.9$. Other details are as decribed in the caption to Fig. 1

14 GeV, $E_T^{\mathrm{jet},2} > 5$ GeV and $-1 < \eta^{\mathrm{jet}} < 2$. The differential dijet cross sections as a function of Q^2 and the invariant mass of the two highest-E_T jets, m_{12}, are presented in Figs. 4 and 5. The NLO QCD calculation gives a good description of the measured dijet cross sections.

7.4 Subjet multiplicities

The mean subjet multiplicity, $\langle n_{\mathrm{sbj}} \rangle$, was determined using the inclusive sample of jets in the kinematic region defined by $Q^2 > 200$ GeV^2 and $y < 0.9$. The $\langle n_{\mathrm{sbj}} \rangle$ values were obtained using every jet of hadrons in the event with $E_T^{\mathrm{jet}} >$ 14 GeV and $-1 < \eta^{\mathrm{jet}} < 2$. The results are shown in Fig. 6 as a function of y_{cut} for different E_T^{jet} regions. In the region of small y_{cut}, the ARIADNE MC model gives a better description of the multiplicity than the NLO QCD calculation MEPJET. At larger values of y_{cut} both the MC model and the NLO QCD calculation give a good

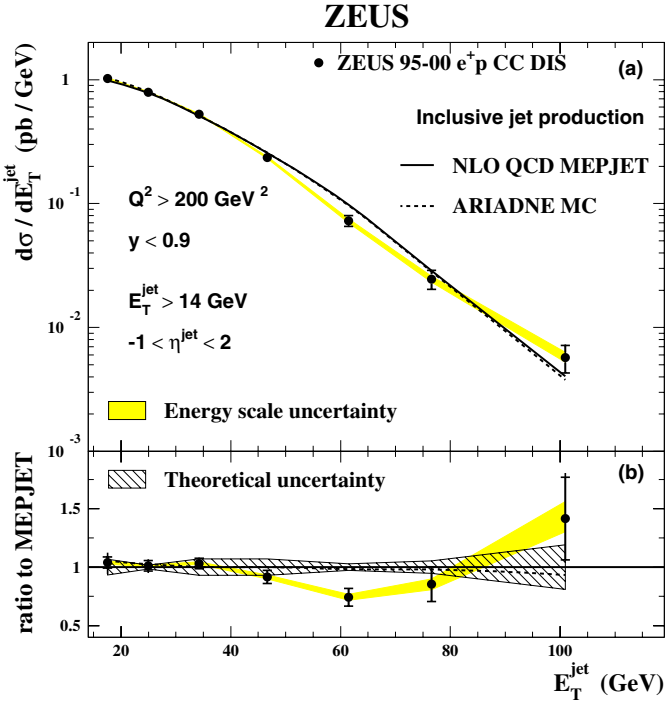

Fig. 3. a The differential cross-section $d\sigma/dE_T^{jet}$ for inclusive jet production in the laboratory frame with $E_T^{jet} > 14$ GeV and $-1 < \eta^{jet} < 2$ in the kinematic region $Q^2 > 200$ GeV ^{2} and $y < 0.9$. Other details are as decribed in the caption to Fig. 1

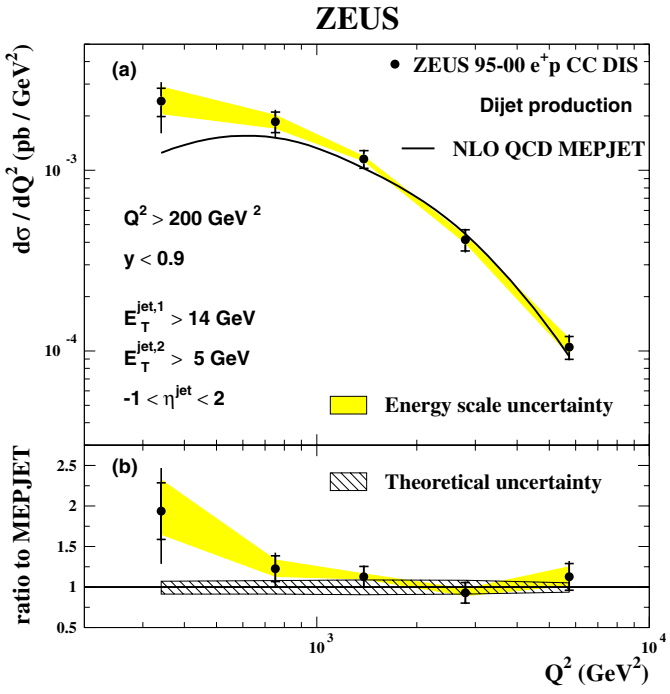

Fig. 4. a The differential cross-section $d\sigma/dQ^2$ for dijet production in the laboratory frame with $E_T^{jet,1} > 14$ GeV, $E_T^{jet,2} > 5$ GeV and $-1 < \eta^{jet} < 2$ in the kinematic region $Q^2 > 200$ GeV ^{2} and $y < 0.9$. Other details are as decribed in the caption to Fig. 1

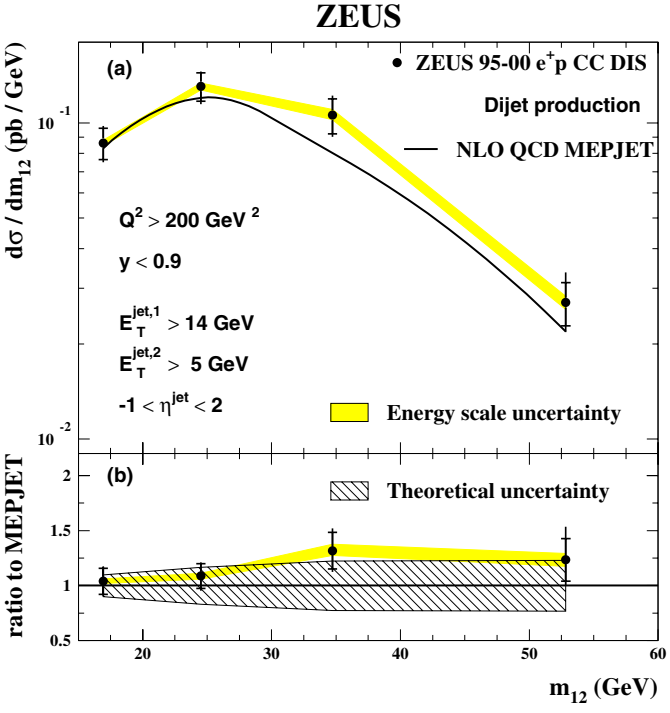

Fig. 5. a The differential cross-section $d\sigma/dm_{12}$ for dijet production in the laboratory frame with $E_T^{jet,1} > 14$ GeV, $E_T^{jet,2} > 5$ GeV and $-1 < \eta^{jet} < 2$ in the kinematic region $Q^2 > 200$ GeV ^{2} and $y < 0.9$. Other details are as decribed in the caption to Fig. 1

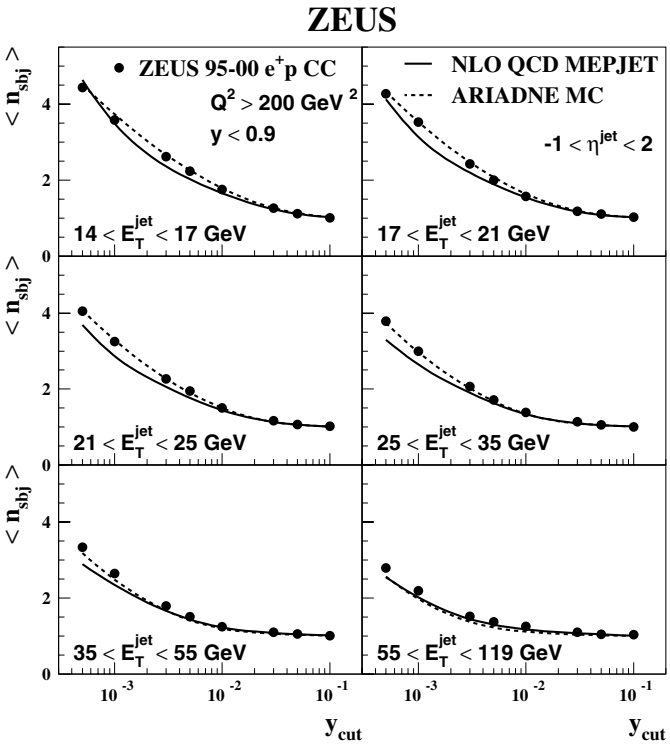

Fig. 6. Mean subjet multiplicity (black dots), $\langle n_{sbj} \rangle$, as a function of y_{cut} for inclusive jet production in the laboratory frame with $-1 < \eta^{jet} < 2$ in different E_T^{jet} regions. The parton shower Monte Carlo prediction given by ARIADNE at hadron level (dashed line) and the next-to-leading-order prediction obtained with MEPJET corrected to hadron level (solid line) are shown. The error bars are smaller than the symbols

description of the measurement. In the region of small $y_{\rm cut}$ values, fixed-order QCD calculations are affected by large uncertainties and a resummation of terms enhanced by $ln(y_{\rm cut})$ [14,15] would be required for a precise comparison with the data. At relatively large values of $y_{\rm cut}$, a NLO fixed-order calculation is expected [14, 15] to be a good approximation to such a resummed calculation.

The measured $\langle n_{\rm sbj} \rangle$ at $y_{\rm cut} = 10^{-2}$ as a function of $E_T^{\rm jet}$ is shown in Fig. 7. The measured mean subjet multiplicity decreases as $E_T^{\rm jet}$ increases. The overall description of the data by the NLO QCD calculations is good.

8 Measurement of α_s

The sensitivity of the subjet multiplicity to the value of $\alpha_s(M_Z)$ is illustrated in Fig. 7, which compares the measured $\langle n_{\rm sbj} \rangle$ at $y_{\rm cut} = 10^{-2}$ as a function of $E_T^{\rm jet}$ with NLO QCD calculations obtained with different values of $\alpha_s(M_Z)$. Both the measurements and the NLO QCD predictions of the subjet multiplicities have smaller uncertainties compared to those of the jet cross sections. Therefore, the measured $\langle n_{\rm sbj} \rangle$, rather than the jet cross sections, was used to determine $\alpha_s(M_Z)$ using the following procedure:

– the NLO QCD calculations of $\langle n_{\rm sbj} \rangle$ were performed for the five sets of the CTEQ4 "A-series" PDFs, which

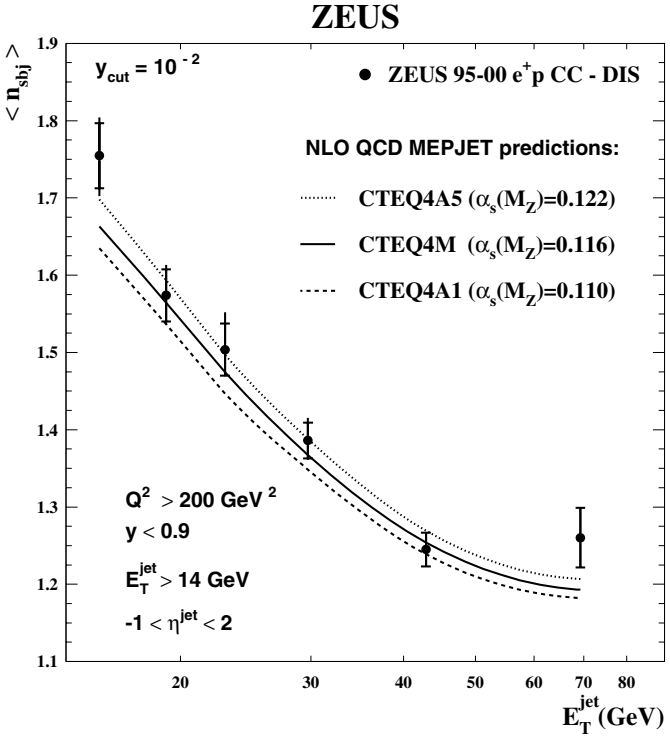

Fig. 7. Mean subjet multiplicity, $\langle n_{sbj} \rangle$, at $y_{cut} = 10^{-2}$ as a function of E_T^{jet} (black dots), for inclusive jet production in the laboratory frame with $E_T^{jet} > 14$ GeV and $-1 < \eta^{jet} < 2$. The inner error bars represent the statistical uncertainty of the data. The outer error bars show the statistical and systematic uncertainties added in quadrature. The NLO QCD predictions obtained with MEPJET using the CTEQ4 sets of proton PDFs are shown for 3 different values of $\alpha_s(M_Z)$ (curves)

differ in the assumed value of $\alpha_s(M_Z)$. The value of $\alpha_s(M_Z)$ used in each calculation was that associated with the corresponding set of PDFs;

– for each bin i in $E_T^{\rm jet}$, the NLO QCD calculations, corrected for hadronisation effects, were used to parametrise the $\alpha_s(M_Z)$ dependence of $\langle n_{\rm sbj} \rangle$ according to

$$[\langle n_{\rm sbj} \rangle(\alpha_s(M_Z))]_i = 1 + C_1^i \alpha_s(M_Z) + C_2^i \alpha_s(M_Z)^2. \quad (3)$$

The coefficients C_1^i and C_2^i were determined by performing a χ^2-fit to the NLO QCD predictions. This simple parametrisation gives a good description of the $\alpha_s(M_Z)$ dependence of $\langle n_{\rm sbj} \rangle$ over the entire range spanned by the CTEQ4 "A-series";

– this parametrisation was used to extract a value of $\alpha_s(M_Z)$ in each bin;

– in addition, a combined value of $\alpha_s(M_Z)$ was determined by a χ^2-fit of Eq. (3) to the measured $\langle n_{\rm sbj} \rangle$ values for all bins.

This procedure correctly handles the complete α_s dependence of the calculations (the explicit dependence coming from the partonic cross sections as well as the implicit dependence coming from the PDFs) in the fit, while preserving the correlation between α_s and the PDFs.

The uncertainty in the extracted values of $\alpha_s(M_Z)$ due to the experimental systematic uncertainties was evaluated by repeating the above analysis for each systematic check. The largest contribution to the experimental uncertainty was that due to the simulation of the hadronic final state.

The theoretical uncertainties arising from terms beyond NLO and uncertainties in the hadronisation correction were evaluated as described in Sect. 5. These resulted in uncertainties in $\alpha_s(M_Z)$ of $\Delta\alpha_s(M_Z) = ^{+0.0064}_{-0.0051}$ and $\Delta\alpha_s(M_Z) = \pm 0.0014$, respectively. The total theoretical uncertainty was obtained by adding these in quadrature. Other uncertainties described in Sect. 5 were small and were neglected. As a cross check, a linear parametrisation of the $\alpha_s(M_Z)$ dependence of $\langle n_{\rm sbj} \rangle$ was considered; the change in the extracted value of $\alpha_s(M_Z)$ was negligible.

The values of $\alpha_s(M_Z)$ obtained from the measurement of $\langle n_{\rm sbj} \rangle$ for various $E_T^{\rm jet}$ regions are in good agreement. The value of $\alpha_s(M_Z)$ obtained from the measurements of $\langle n_{\rm sbj} \rangle$ at $y_{\rm cut} = 10^{-2}$ for $25 < E_T^{\rm jet} < 119$ GeV, a region in which the parton-to-hadron correction was less than 10%, is

$$\alpha_s(M_Z) = 0.1202 \pm 0.0052({\rm stat.})^{+0.0060}_{-0.0019}({\rm syst.})^{+0.0065}_{-0.0053}({\rm th.}).$$

This result is consistent with other recent determinations using measurements in NC DIS of inclusive jet [61,62] and exclusive dijet cross sections [63] as well as measurements of $\langle n_{\rm sbj} \rangle$ [18] and with the PDG value, $\alpha_s(M_Z) = 0.1172 \pm 0.0020$ [64].

9 Comparison of subjet multiplicities in CC and NC

The present measurements of subjet multiplicities in CC interactions are compared with the corresponding measurements in NC DIS [18]. The NC data were reanalysed in the same kinematic region as that of the CC analysis.

The measurements of $\langle n_{\rm sbj} \rangle$ at the value of $y_{\rm cut} = 10^{-2}$ as a function of $E_T^{\rm jet}$ in CC and NC DIS are compared in Fig. 8a. The value of $\langle n_{\rm sbj} \rangle$ is slightly larger for jets in NC DIS than for CC DIS for a given jet transverse energy. The NLO QCD predictions behave in the same way as the data.

The subprocess population and the phase space available for QCD radiation depend on Q^2. The measurements of $\langle n_{\rm sbj} \rangle$ at $y_{\rm cut} = 10^{-2}$ as a function of Q^2 in CC and NC DIS are compared in Fig. 8b. The values of $\langle n_{\rm sbj} \rangle$ in CC and NC DIS are similar and are in agreement with the NLO predictions. The differences observed in the subjet multiplicity as a function of $E_T^{\rm jet}$ can be attributed to the different Q^2 distributions of the CC and NC processes.

10 Summary

Measurements of differential cross sections for inclusive jet and dijet production in charged current deep inelastic e^+p scattering have been performed and are corrected to the electroweak Born level. The internal structure of the inclusive jet sample has been studied in terms of the

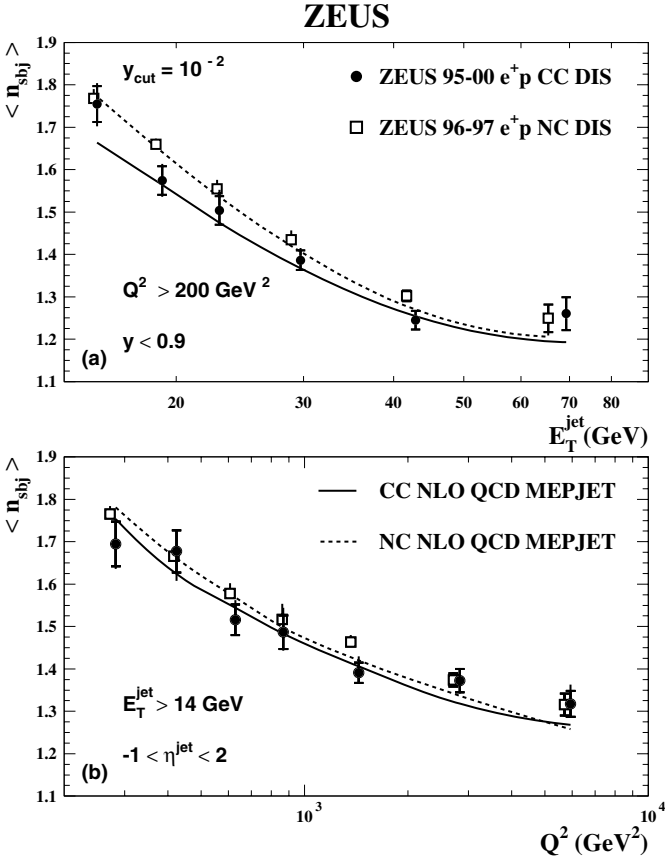

Fig. 8. Measurements of $\langle n_{\rm sbj} \rangle$ at $y_{cut} = 10^{-2}$ for inclusive jet production in the laboratory frame with $E_T^{jet} > 14$ GeV and $-1 < \eta^{jet} < 2$ in charged current DIS (circles) and neutral current DIS (open squares) as a function of **a** E_T^{jet} and **b** Q^2

mean subjet multiplicity. The results are given for jets of hadrons identified with the longitudinally invariant k_T cluster algorithm in the laboratory frame in the kinematic region defined by $Q^2 > 200$ GeV^2 and $y < 0.9$. Inclusive jet cross sections are presented for jets with transverse energies $E_T^{\rm jet} > 14$ GeV and pseudorapidities in the range $-1 < \eta^{\rm jet} < 2$. Dijet cross sections are presented for events with a jet having $E_T^{\rm jet} > 14$ GeV and a second jet having $E_T^{\rm jet} > 5$ GeV.

The predictions of the ARIADNE MC model and NLO QCD calculations obtained with the program MEPJET give a good description of the measurements of inclusive and dijet cross sections.

The average number of subjets decreases as $E_T^{\rm jet}$ increases. The NLO QCD calculations agree well with the measured subjet multiplicities, $\langle n_{\rm sbj} \rangle$. A fit of the measured $\langle n_{\rm sbj} \rangle$ as a function of $E_T^{\rm jet}$ at $y_{\rm cut} = 10^{-2}$ provides a determination of the strong coupling constant $\alpha_s(M_Z)$. The value of $\alpha_s(M_Z)$ determined for the region $E_T^{\rm jet} > 25$ GeV is

$$\alpha_s(M_Z) = 0.1202 \pm 0.0052({\rm stat.})^{+0.0060}_{-0.0019}({\rm syst.})^{+0.0065}_{-0.0053}({\rm th.}).$$

This result is consistent with other recent determinations and with the PDG value.

The subjet multiplicities in CC and NC DIS are similar as a function of Q^2. The measured $\langle n_{\rm sbj} \rangle$ at a given $E_T^{\rm jet}$ is somewhat smaller in CC DIS than in NC DIS. This can be attributed to the different Q^2 distributions of the two processes.

Acknowledgements. We thank the DESY Directorate for their strong support and encouragement. The remarkable achievements of the HERA machine group were essential for the successful completion of this work and are greatly appreciated. We are grateful for the support of the DESY computing and network services. The design, construction and installation of the ZEUS detector have been made possible owing to the ingenuity and effort of many people who are not listed as authors. We would like to thank D. Zeppenfeld for useful discussions and help in running his program for calculating QCD jet cross sections in charged current interactions.

References

1. H1 Collaboration, T. Ahmed et al., Phys. Lett. B **324**, 241 (1994)
2. ZEUS Collaboration, M. Derrick et al., Phys. Rev. Lett. **75**, 1006 (1995)
3. H1 Collaboration, S. Aid et al., Z. Phys. C **67**, 565 (1995)
4. H1 Collaboration, S. Aid et al., Phys. Lett. B **379**, 319 (1996)
5. ZEUS Collaboration, M. Derrick et al., Z. Phys. C **72**, 47 (1996)
6. ZEUS Collaboration, J. Breitweg et al., Eur. Phys. J. C **12**, 411 (2000); Erratum in Eur. Phys. J. C **27**, 305 (2003)
7. ZEUS Collaboration, S. Chekanov et al., Phys. Lett. B **539**, 197 (2002); Erratum in Phys. Lett. B **552**, 308 (2003)
8. H1 Collaboration, C. Adloff et al., Eur. Phys. J. C **13**, 609 (2000)
9. H1 Collaboration, C. Adloff et al., Eur. Phys. J. C **19**, 269 (2001)
10. H1 Collaboration, C. Adloff et al., Eur. Phys. J. C **19**, 429 (2001)
11. ZEUS Collaboration, J. Breitweg et al., Eur. Phys. J. C **8**, 367 (1999)
12. S. Catani et al., Nucl. Phys. B **383**, 419 (1992)
13. M.H. Seymour, Phys. Lett. B **378**, 279 (1996)
14. M.H. Seymour, Nucl. Phys. B **421**, 545 (1994)
15. J.R. Forshaw and M.H. Seymour, JHEP **9909**, 009 (1999)
16. S. Catani et al., Nucl. Phys. B **406**, 187 (1993)
17. J.G. Körner, E. Mirkes and G.A. Schuler, Int. J. Mod. Phys. A **4**, 1781 (1989)
18. ZEUS Collaboration, S. Chekanov et al., Phys. Lett. B **558**, 41 (2003)
19. ZEUS Collaboration, U. Holm (ed.), The ZEUS Detector. Status Report (unpublished), DESY (1993), available on `http://www-zeus.desy.de/bluebook/bluebook.html`
20. N. Harnew et al., Nucl. Instr. and Meth. A **279**, 290 (1989)
21. B. Foster et al., Nucl. Phys. Proc. Suppl. B **32**, 181 (1993)
22. B. Foster et al., Nucl. Instr. and Meth. A **338**, 254 (1994)
23. M. Derrick et al., Nucl. Instr. and Meth. A **309**, 77 (1991)
24. A. Andresen et al., Nucl. Instr. and Meth. A **309**, 101 (1991)
25. A. Caldwell et al., Nucl. Instr. and Meth. A **321**, 356 (1992)

26. A. Bernstein et al., Nucl. Instr. and Meth. A **336**, 23 (1993)
27. W.H. Smith, K. Tokushuku and L.W. Wiggers, Proc. Computing in High-Energy Physics (CHEP), Annecy, France, Sept. 1992, C. Verkerk and W. Wojcik (eds.), p. 222. CERN (1992); also in preprint DESY92-150B
28. J. Andruszków et al., Preprint DESY-92-066, DESY, 1992
29. ZEUS Collaboration, M. Derrick et al., Z. Phys. C **63**, 391 (1994)
30. J. Andruszków et al., Acta Phys. Pol. B **32**, 2025 (2001)
31. F. Jacquet and A. Blondel, Proc. of the Study of an *ep* Facility for Europe, U. Amaldi (ed.), p. 391. Hamburg, Germany (1979); also in preprint DESY 79/48
32. S.D. Ellis and D.E. Soper, Phys. Rev. D **48**, 3160 (1993)
33. J.E. Huth et al., Research Directions for the Decade. Proc. of Summer Study on High Energy Physics, 1990, E.L. Berger (ed.), p. 134. World Scientific (1992); also in preprint FERMILAB-CONF-90-249-E
34. G. Ingelman, A. Edin and J. Rathsman, Comp. Phys. Comm. **101**, 108 (1997)
35. A. Kwiatkowski, H. Spiesberger and H.-J. Möhring, Comp. Phys. Comm. **69**, 155 (1992)
36. H. Spiesberger, An Event Generator for *ep* Interactions at HERA Including Radiative Processes (Version 4.6), 1996, available on `http://www.desy.de/~hspiesb/heracles.html`
37. K. Charchula, G.A. Schuler and H. Spiesberger, Comp. Phys. Comm. **81**, 381 (1994)
38. H. Spiesberger, HERACLES and DJANGOH: Event Generation for *ep* Interactions at HERA Including Radiative Processes, 1998, available on `http://www.desy.de/~hspiesb/djangoh.html`
39. H.L. Lai et al., Phys. Rev. D **55**, 1280 (1997)
40. Y. Azimov et al., Phys. Lett. B **165**, 147 (1985)
41. G. Gustafson, Phys. Lett. B **175**, 453 (1986)
42. G. Gustafson and U. Pettersson, Nucl. Phys. B **306**, 746 (1988)
43. B. Andersson et al., Z. Phys. C **43**, 625 (1989)
44. L. Lönnblad, Comp. Phys. Comm. **71**, 15 (1992)
45. L. Lönnblad, Z. Phys. C **65**, 285 (1995)
46. ZEUS Collaboration, J. Breitweg et al., Eur. Phys. J. C **11**, 251 (1999)
47. B. Andersson et al., Phys. Rep. **97**, 31 (1983)
48. T. Sjöstrand, Comp. Phys. Comm. **39**, 347 (1986)
49. T. Sjöstrand and M. Bengtsson, Comp. Phys. Comm. **43**, 367 (1987)
50. R. Brun et al., GEANT3, Technical Report CERN-DD/EE/84-1, CERN, 1987
51. M. Vázquez. Ph.D. Thesis, Universidad Autónoma de Madrid, Report DESY-THESIS-2003-006, 2003 (unpublished)
52. E. Mirkes and D. Zeppenfeld, Phys. Lett. B **380**, 205 (1996)
53. W.T. Giele and E.W. Glover, Phys. Rev. D **46**, 1980 (1992)
54. H.L. Lai et al., Eur. Phys. J. C **12**, 375 (2000)
55. A.D. Martin et al., Eur. Phys. J. C **4**, 463 (1998)
56. A.D. Martin et al., Eur. Phys. J. C **14**, 133 (2000)
57. ZEUS Collaboration, S. Chekanov et al., Phys. Lett. B **531**, 9 (2002)
58. ZEUS Collaboration, S. Chekanov et al., Eur. Phys. J. C **23**, 615 (2002)
59. M. Wing (on behalf of the ZEUS Collaboration), in Proc. for "10th International Conference on Calorimetry in High Energy Physics", 2002, R. Zhu (ed.), p. 767, Pasadena, USA, 2002; also in hep-ex/0206036
60. Particle Data Group, D.E. Groom et al., Eur. Phys. J. C **15**, 1 (2000)
61. ZEUS Collaboration, S. Chekanov et al., Phys. Lett. B **547**, 164 (2002)
62. H1 Collaboration, C. Adloff et al., Eur. Phys. J. C **19**, 289 (2001)
63. ZEUS Collaboration, J. Breitweg et al., Phys. Lett. B **507**, 70 (2001)
64. Particle Data Group, K. Hagiwara et al., Phys. Rev. D **66**, 010001 (2002)